



An Evaluation of the Shielding Effectiveness of Tellurite Glass with Composition $85\text{TeO}_2\text{-}5\text{Nb}_2\text{O}_5\text{-}5\text{ZnO-}5\text{Ag}_2\text{O}$ for Diagnostic Radiology Application

Khalid I. Hussein^{1,2*}

¹*Department of Radiological Sciences, College of Applied Medical Sciences, King Khalid University, Abha 61421, Saudi Arabia.*

²*Department of Medical Physics and Instrumentation, National Cancer Institute, University of Gezira, Wad Medani 20, Sudan, North Africa.*

Author's contribution

The sole author designed, analysed, interpreted and prepared the manuscript.

Article Information

DOI: 10.9734/CJAST/2021/v40i731330

Editor(s):

(1) Dr. Orlando Manuel da Costa Gomes, Lisbon Polytechnic Institute, Portugal.

Reviewers:

(1) Juniastel Rajagukguk, Universitas Negeri Medan, Indonesia.

(2) Shaik Kareem Ahmmad, Muffakham Jah College of Engineering and Technology, India.

(3) Boora Srinivas, VNR Vignana Jyothi Institute of Engineering and Technology, India.

Complete Peer review History: <http://www.sdiarticle4.com/review-history/67962>

Received 18 February 2021

Accepted 27 April 2021

Published 30 April 2021

Original Research Article

ABSTRACT

The metal oxide glasses have attracted huge interest as promising types of shielding materials to replace the toxic, heavy and costly conventional shielding materials. In this work, the physical and the shielding effectiveness of Tellurite glass sample (S1) contain host metal oxides ($85\text{TeO}_2\text{-}5\text{Nb}_2\text{O}_5\text{-}5\text{ZnO-}5\text{Ag}_2\text{O}$) were evaluated at photon energies range between 15keV and 1MeV. The shielding parameters of the proposed glass system such as linear attenuation coefficients, HVL, MFP, Z_{eff} , and N_{eff} were evaluated. The proposed samples showed a superior performance at the diagnostic energy range between 40 and 90 keV and a comparable shielding effectiveness above 90keV when compared with other commercial standard shielding materials.

Keywords: *Tellurite glasses; mass attenuation coefficient; linear attenuation coefficient; half-value layer; mean free path; radiation shielding.*

*Corresponding author: E-mail: kirahim@kku.edu.sa;

1. INTRODUCTION

Since the discovery of x-ray by Roentgen in 1895 and the radioactivity by Henri Becquerel in 1896, the radiation applications such as nuclear power, medical imaging, cancer treatment and nuclear engineering are dramatically increased over the past decades [1-3]. The improper use of radiation can lead to serious injuries. The severity of radiation injuries depends on the radiation exposure dose rate. The radiation risk and injuries in different application were widely addressed by several researcher [4-8].

The use of ionizing radiation required safety standards to be establish and implement to ensure the protection of people and environment, many standards for radiation protection and safety were established [9-12]. Exposure time, distance from the source and shielding are the basic principles of protection considered when dealing with ionizing radiation. Shielding is most important consideration for any facility that perform diagnostic or therapy procedures. Many factors affecting the effectiveness of a shielding materials used to protect people working in radiation facilities such radiation energy, radiation type, the thickness of shielding material. The denser the material the more effective shielding materials against X-rays and gamma rays. Lead is the most common material use in most of radiation applications as shielding material due to its high atomic number. Although, lead is the most effective material in attenuating gamma and X-ray photons but can cause pollution through release of lead particles and can affected all the system body [13-14].

Due to the toxicity, high cost, and heavy weight of lead and lead glass materials several studies were conducted to develop alternative materials that replace lead such as tellurite-base glasses, phosphate-based materials, metal alloy, polymers [15-28]. These studies showed a good shielding performance in terms of high shielding efficiency without loss of transparency, good physical properties, thermal stability and good optical properties.

The shielding effectiveness have been studies in terms of the physical properties, radiation

shielding parameters, LAC, MAC, HVL, MFP, Zeff and Neff. Al-Hadeethi et.al [24] have studied the x-ray photons attenuation characteristics for two glass-based systems (Bi_2O_3 - B_2O_3 - TeO_2 - TiO_3 and PbO - ZnO - TeO_2 - B_2O_3) at photon energies ranging from 30 to 80kVp. Their results showed that the increase of Tellurium dioxide (TeO_2) concentration increases the attenuation coefficients of the glasses system with a decrease in the half-value layer especially at photon energy range between 70 and 80keV. Mhared et.al [25] have studied the shielding effectiveness of lithium-magnesium-borate glasses with Thulium oxide (Tm_2O_3). Their results showed that the attenuation coefficients increase with increasing Tm_2O_3 concentration. Lakshminarayana et.al [26] have studied the radiation shielding effectiveness of borosilicate glasses doped Tm^{3+} ions for gamma application. Their results indicates that the sample contain highest mole concentration of Tm_2O_3 has the greater ability to attenuate gamma-rays.

In this work, the shielding effectiveness of Tellurite based-glass sample (S1) was investigated at photon energy range between 15keV and 1MeV. The radiation shielding parameters of the prepared glass system such as LAC, MAC, HVL, Z_{eff} , Z_{eq} , MFP, N_{eff} and EBF were calculated using the online developed software (Phy-X/PSD) [27]. The results of shielding parameters were compared with other commercial shielding materials commonly used in photon applications.

2. THEORY AND METHOD

Tellurite glasses samples contain different oxides(S1) (85TeO_2 - $5\text{Nb}_2\text{O}_5$ - 5ZnO - $5\text{Ag}_2\text{O}$) were prepared by putting the raw material in Platinum crucible in the heating furnace at a temperature in range from 850 to 950 °C for 30 min. The melting material was stirred to increase the viscosity before cast in the brass mold. The prepared sample was put in the annealing furnace for 2h at 320 °C. The sample density was measured using Archimedes' Principle. Table1 shows the density, molar weight (MW) and the chemical compositions of the prepared sample.

Table 1. The Physical parameters and chemical compositions of the proposed glass (S1)

Sample code	Mw(g/mol)	Density(g/cm ³) ±0.04	Composition (mol%)			
			TeO ₂	Nb ₂ O ₅	ZnO	Ag ₂ O
S1	164.61	5.3744	85	5	5	5

The average molar weight of mixtures \bar{M} can be calculated using mole by fractions x_i and molar masses M_i of the constituent elements of the component and their [28]:

$$\bar{M} = \sum x_i M_i \quad (1)$$

where x_i is the molar fraction of each component i , M_i is the molecular weight of the sample.

The molar volume (V_M) of glass material can be calculated by the following equation [28]:

$$V_M = \frac{\bar{M}}{\rho} \quad (2)$$

Where M is the average molar weight of the sample, ρ is the density of the sample.

$$OPD = 1000 \sum x_i n_i \left(\frac{1}{V_M} \right) \quad (3)$$

where V_M is the molar volume of the glass materials, x_i is a molar fraction, n_i is the number of oxygen atoms in each oxide. The molar refraction of R_m can be calculated using the following equation [28]:

$$R_m = \frac{n^2-1}{n^2+2} \times V_m \quad (4)$$

The reflection loss, R_L in percentage, can be calculated using the following equation [28]:

$$R_L = \left[\frac{(n-1)}{(n+1)} \right]^2 \quad (5)$$

where n is the refractive index of the glass materials. The molar electronic polarizability (α_m) can be calculated using the following equation [28]:

$$\alpha_m = \frac{R_m}{2.52} \quad (6)$$

The ionic concentrations of the glass samples are determined using the following relation [29]:

$$N = \frac{\text{mol \% of Te} \times \text{glass density} \times \text{Avogadro's number}}{\text{Average molecular weight of glass}} \quad (\text{ion/cm}^3) \quad (7)$$

The polaron radius was calculated using the formula [29]:

$$r_p = \frac{1}{2} \left(\frac{\pi}{6N} \right)^{1/3} \quad (8)$$

Where N is the ionic concentrations.

Inter-ionic distance of the glass samples is given as [29]:

$$r_i = \left(\frac{1}{N} \right)^{1/3} \quad (9)$$

Where r_i is the ionic concentrations.

The effectiveness of a shielding material can be investigated by the physical properties and radiation shielding parameters. The MAN, LAC, Zeff, Neff, HVL and MFP are the most important radiation shielding parameters that characterizing the effectiveness of the shielding materials. The cross section for scattering and absorption can be express in term of the total mass attenuation coefficient (μ/ρ), which can be calculated using the program Xcom [30]. The mass attenuation coefficient of a compound can be computed using the following relation [30-34]:

$$\frac{\mu}{\rho} = \sum_i w_i \left(\frac{\mu}{\rho} \right)_i \quad (10)$$

Where w_i is the fraction by weight of the i th atomic element and $\left(\frac{\mu}{\rho} \right)_i$ is the mass attenuation of the of the i^{th} atomic element.

The probability of photon interaction with material can be characterized by the total atom cross-section (σ_a) and total electronic cross-section (σ_e) using the following relations [33-34]:

$$\sigma_a = \frac{1}{N_A} \sum_i f_i A_i \left(\frac{\mu}{\rho} \right)_i \quad (11)$$

$$\sigma_e = \frac{1}{N_A} \sum_j f_j \frac{A_j}{Z_j} \left(\frac{\mu}{\rho} \right)_j \quad (12)$$

Where f_i is fraction by mole of the i th atomic element, A_i is atomic weight of the i th atomic element, Z_j is atomic number and N_A is Avogadro constant.

The effective atomic number which varies with energies can be calculated from the ratio of atomic and electronic cross-sections by the following relation [33-34]:

$$Z_{\text{eff}} = \frac{\sigma_a}{\sigma_e} \quad (13)$$

The effective electron number (Neff) is representing the number of electrons per unit mass of the shielding material can be computed using the following relation [33-34]:

$$N_e = \frac{N_A}{A} Z_{\text{eff}} \quad (14)$$

Where A is the mean atomic mass equal to $\sum_i f_i A_i$; f_i is fraction by mole of the i th atomic

element, A_i is atomic weight of the i th atomic element.

The half-value layer (HVL) and the mean free pass (MFP) are considered as important parameters for the estimation of the required effective shielding thickness for each photon energy. The HVL is the required thickness to reduce radiation intensity of the mono-energetic beam to its half value, while the MFP is representing the average distance between two successive interaction. These parameters can be computed according to the following relations [33-34]:

$$HVL = \frac{0.693}{\mu} \tag{15}$$

$$MFP = \frac{1}{\mu} \tag{16}$$

Where μ is the linear attenuation coefficient.

3. RESULTS AND DISCUSSION

Table 2 and 3 illustrate the calculated ion concentration, polaron radius, inter-ionic

distance, oxygen packing density (OPD), the molar refraction (R_m) and the molar electronic polarizability (α_m) of the prepared sample. As shown in Table 2, the smaller values recorded for the polaron radius and inter-ionic distance indicate an increase in polarizability, which leads to an increase in electrical conductivity of prepared glass system [29,35]. Table 3 shows comparison between the prepared glass sample and some commercially available glass shielding materials such as that developed by Schott Co., Germany standard shielding glass materials (RS 253-G18, RS 520 and RS 360) [36]. As shown in Table 3, the prepared sample recorded the highest values compared to the other glass systems. This indicates that the proposed glass has more non-bridging oxygen, which improve the stability of glass as host matrix for rare earth elements.

Fig. 1 shows the XRD pattern of prepared glasses. As shown in Fig. 1, the XRD pattern abroad defused scattering in 2θ range between 20 and 30, which indicate the amorphous glass nature of the prepared sample.

Table 2. The Tellurite ion concentration, polaron radius, and inter ionic distance

The concentration ($N \times 10^{21}$), ions/cm ³ (± 0.01)	1.67
Polaron radius ($r_p \times 10^{-8}$), Å (± 0.01)	1.576
Inter ionic distance ($r_i \times 10^{-7}$), Å (± 0.01)	3.911

Table 3. The OPD, R_m and α_m of the prepared sample prepared sample compared with RS 253-G18, RS 520 and RS 360 standard materials

Sample code	Refractive Index	OPD (mol/l)	R_m (m3)	α_m (x10-24.cm3)
S1	2.10	66.93	16.62	6.60
RS253 G18	1.52	71.18	8.20	3.25
RS360	1.62	38.22	13.32	5.29
RS520	1.81	37.45	14.62	5.80

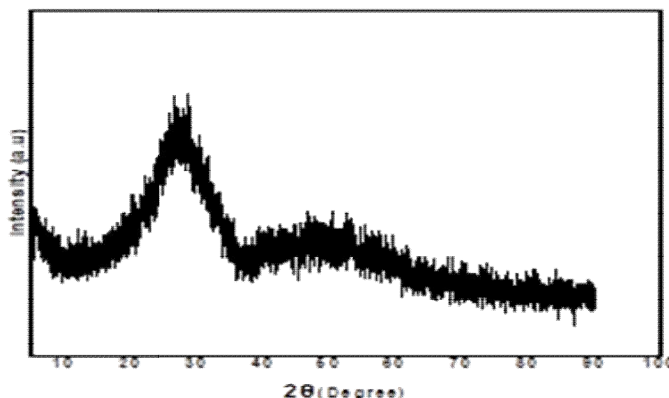


Fig. 1. XRD pattern of prepared glass

Fig. 2A and 2B show the computed linear attenuation coefficients (LAC) of the prepared sample (85TeO₂-5Nb₂O₅-5ZnO-5Ag₂O) and some of the common commercial standard materials; RS 253-G18, RS 360, RS 520, Chromite, Chromite, Ferrite, Magnetite and Barite at energy range between 15keV and1MeV. The LAC for the prepared glass sample were computed using the online developed software (Phy-X/PSD) [27]. The prepared sample recorded the highest values in the energies ranging from 40keV to 90keV as shown in Fig. 2A and 2B. For example, the value of linear attenuation coefficient recorded for the prepared sample was 13.29cm⁻¹ compared to 1.148, 6.19, 10.63, 2.11, 2.45, 2.47 and 10.86cm⁻¹ at 80keV, with percentage differences of 91.36%, 53.46%, 20%, 84.13% and 81.60%, 81.40% and 18.29 for RS 253-G18, RS 360, RS 520, Chromite, Chromite, Ferrite, Magnetite and Barite respectively. Above 90keV the prepared glass material recorded higher values than RS 253-G18, Chromite, Chromite, Ferrite, Magnetite and Barite, while the other standard glasses materials RS-520, RS-360 recorded slightly higher values than the prepared glass sample. The superiority of the prepared sample over all standard materials in the diagnostic energy range (40 to 90keV) is due to the fact that Tellurite glass doped with suitable modifier provide more bridging oxygen as host glass network, in addition to thermal stability, durability and good optical properties. These results are consistent with other findings [19, 20, 21].

compared with some commercially available shielding materials such as Schott Co. Germany standard shielding glass materials (RS 253-G18, RS 360, RS520) [36] and some of the common oxide used with concrete materials such as Chromite, Ferrite, Magnetite and Barite [37], at energy range between 15keV and1MeV. As shown in the Fig. 3A and 3B the recorded HVL values of the sample is lower than the commercially available shielding materials in the energy range between 15keV and 90keV, which is expected due to the higher linear attenuation recorded for prepared sample compared with standard materials. For example, the computed MFP value of S1 was 0.052cm compared to 0.604, 0.056, 0.112, 0.065, 0.329, 0.281 and 0.064cm at 80keV, with percentage differences of 168.3%, 7.4%, 73.1%, 22.2%, 145.4% and 20.7% for the RS 253-G18,RS 360, RS 520, Chromite, Chromite, Ferrite, Magnetite and Barite respectively. The low recorded values are due to the high molecular weight and density of the prepared glass compared with the other standard materials. Above 90keV the prepared glass material shows superior effectiveness over RS 253-G18, Chromite, Chromite, Ferrite, Magnetite and Barite, while the other standard glasses materials RS-520, RS-360 recorded slightly lower values than the prepared glass sample.

As shown in Fig. 4A and 4Bthe prepared sample also recorded the lowest values of MFP compare with the RS 253-G18, Chromite, Chromite, Ferrite, Magnetite and Barite, and slightly higher than RS-520 and RS-360.

Fig. 3A and 3B show the computed half-value layers (HVL) of the prepared sample (S1)

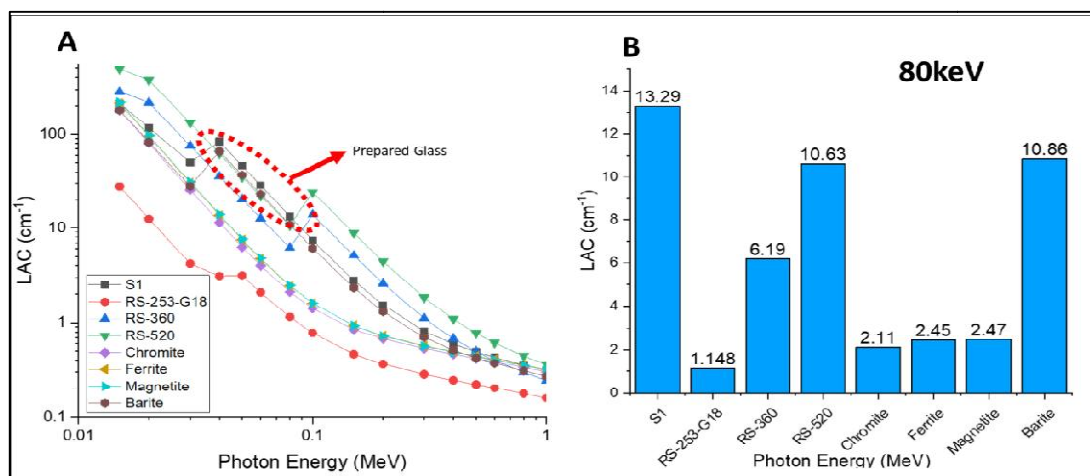


Fig. 2. The LAC for proposed glass sample (S1) compared with some common commercial shielding materials; at photon energy range between 15Kev and1MeV(A); 80keV (B)

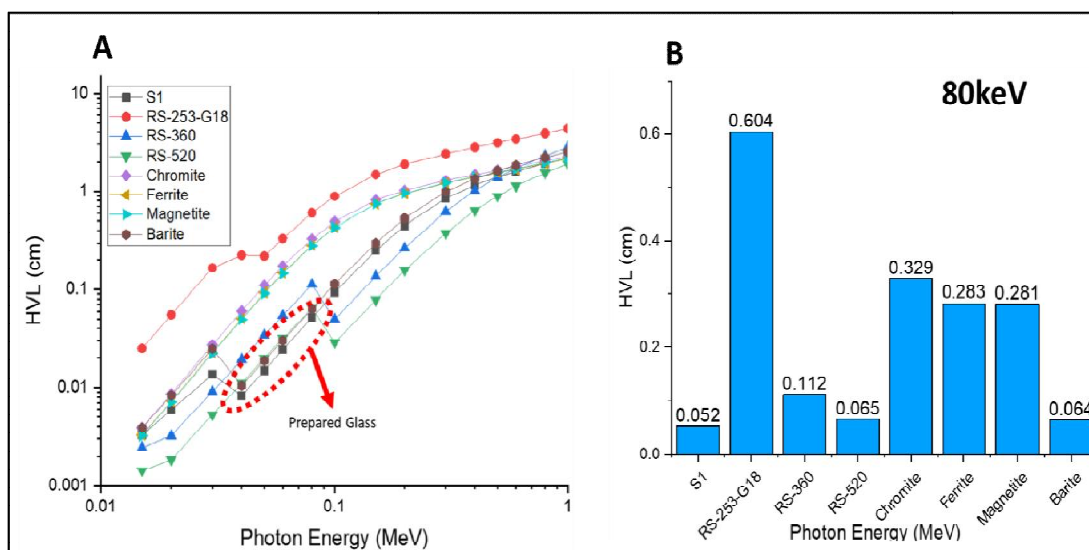


Fig. 3. The HVL for proposed glass sample (S1) compared with some common commercial shielding materials; at photon energy range between 15Kev and 1MeV (A); 80keV (B)

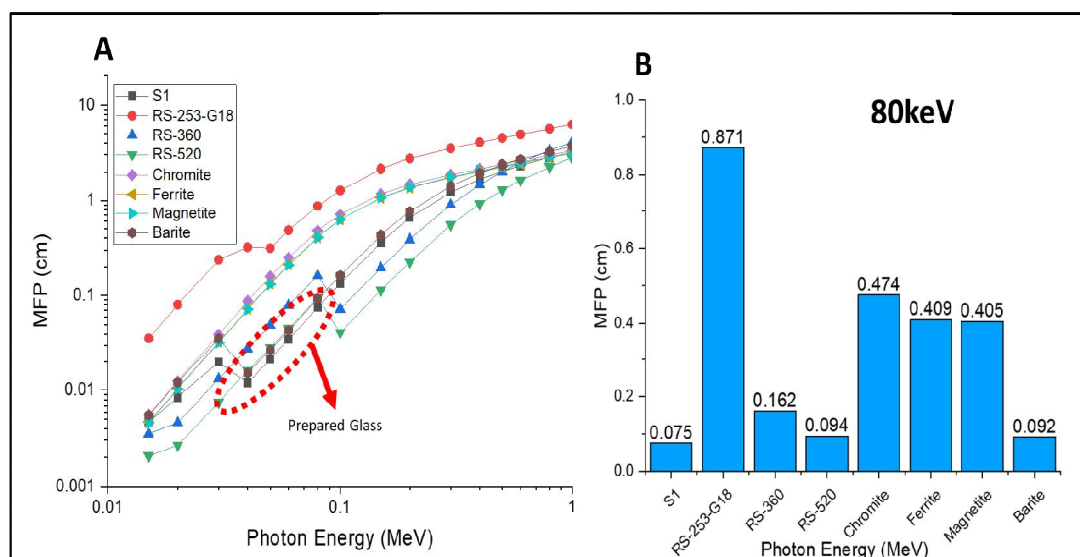


Fig. 4. The MFP for proposed glass sample (S1) compared with some common commercial shielding materials; at photon energy range between 15Kev and 1MeV (A); 80keV (B)

Fig. 5A and 5B shows the values of the total atom cross-section (σ_a) and total electronic cross-section (σ_e) as a function of photon energy for the prepared sample material compared with the commercially available shielding materials. The prepared sample recorded the higher values of σ_a and σ_e at diagnostic energy range.

Fig. 6A and 6B illustrated the effective atomic number (Z_{eff}) and effective electron numbers (N_{eff}) against photon energy (MeV) of the

prepared glass sample. The radiation shielding values recorded for the prepared sample are comparable to the values provided for commercially available shielding materials. The maximum Z_{eff} value of 49 was recorded at energy 40keV, while the minimum value of 23.1 is recorded at energy 1MeV, which indicates the better efficiency of the sample as a shielding material compare with the other samples. These results consistent with findings discussed before for linear attenuations.

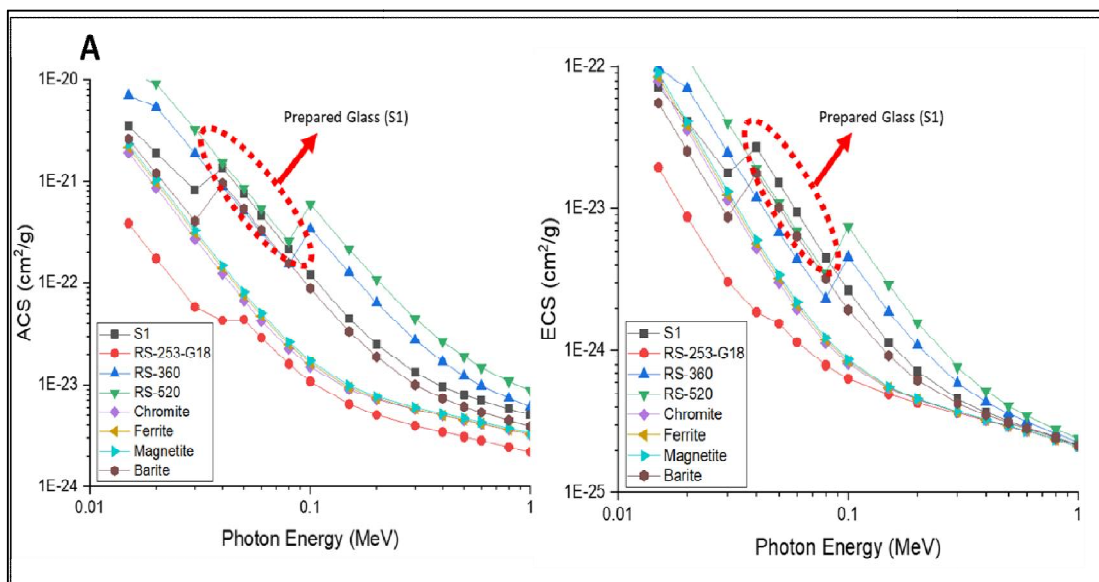


Fig. 5. The ACS (A) and ECS (B) of proposed sample (S1) compared with standard materials at photon energy range between 15keV and 1MeV

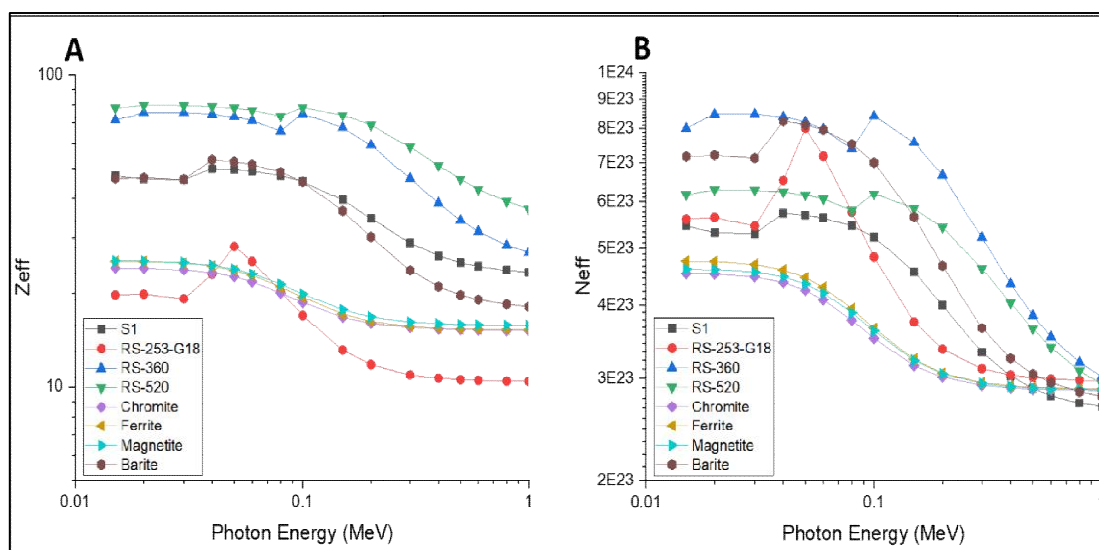


Fig. 6. The Z_{eff} (A) and the N_{eff} (B) of proposed sample (S1) compared with standard materials at photon energy range between 15keV and 1MeV

4. CONCLUSION

Shielding and physical properties of a tellurite glass sample contain host metal oxides ($85TeO_2-5Nb_2O_5-5ZnO-5Ag_2O$) were evaluated at photon energies range between 15keV and 1MeV. The shielding parameters of the proposed glass system such as linear attenuation coefficients, HVL, MFP, Z_{eff} , and N_{eff} were evaluated. The proposed samples showed a superior

performance at the diagnostic energy range between 40 and 90 keV and a comparable shielding effectiveness above 90keV when compared with other commercial standard shielding materials. Each of the metal oxide selected for the preparation of the proposed glass material has its unique properties in term of the good physical, optical and shielding properties such as glass formation, thermal, radiation shielding effectiveness and

transparency, which make the prepared sample a promising glass material not only for shielding purposes but also for other medical applications.

COMPETING INTERESTS

Author has declared that no competing interests exist.

REFERENCES

1. Parker HMOD, Joyce MJ. The use of ionizing radiation to image nuclear fuel: A review. *Progress in Nuclear Energy*. 2015;85:297-318.
2. Vreysen MJB, Robinson AS. Ionising Radiation and Area-Wide Management of Insect Pests to Promote Sustainable Agriculture. 2011;671-92.
3. Smith-Bindman R, Miglioretti DL, Larson EB. Rising use of diagnostic medical imaging in a large integrated health system. *Health Aff (Millwood)*. 2008;27(6):1491-502.
4. Johanna M Meulepas, Cécile M Ronckers, Anne M J B Smets, Rutger A J Nievelstein, Patrycja Gradowska, Choonsik Lee, Andreas Jahnen, Marcel van Straten, Marie-Claire Y de Wit, Bernard Zonnenberg, Willemijn M Klein, Johannes H Merks, Otto Visser, Flora E van Leeuwen, Michael Hauptmann. Radiation exposure from pediatric ct scans and subsequent cancer risk in the Netherlands. *JNCI: Journal of the National Cancer Institute*; 2018. DOI: 10.1093/jnci/djy104.
5. Mathews JD, Forsythe AV, Brady Z, et al. Cancer risk in 680,000 people exposed to computed tomography scans in childhood or adolescence: Data linkage study of 11 million Australians. *BMJ*. 2013;346:f2360. Published 2013 May 21. DOI: 10.1136/bmj.f2360
6. Linet MS, Slovis TL, Miller DL, et al. Cancer risks associated with external radiation from diagnostic imaging procedures [published correction appears in *CA Cancer J Clin*. 2012 Jul-Aug;62(4):277]. *CA Cancer J Clin*. 2012; 62(2):75-100. DOI: 10.3322/caac.21132
7. Hall EJ, Brenner DJ. Cancer risks from diagnostic radiology: The impact of new epidemiological data. *Br J Radiol*. 2012; 85(1020):e1316-e1317. DOI: 10.1259/bjr/13739950
8. Washington: National Academies Press. Committee to assess health risks from exposure to low levels of ionizing radiation NRC. Health risks from exposure to low levels of ionizing radiation: BEIR VII Phase 2; 2006.
9. Radiation Protection and Safety in Medical Uses of Ionizing Radiation, IAEA Safety Standards for protecting people and the environment, Specific Safety Guide No. SSG-46. International atomic energy agency (IAEA). Vienna, 2018. Available: https://www-pub.iaea.org/MTCD/Publications/PDF/PUB1775_web.pdf
10. International atomic energy agency (IAEA), Justification of Practices, Including Non-medical Human Imaging, IAEA Safety Standards Series No. GSG-5, IAEA, Vienna; 2014.
11. International commission on radiation protection. The 2007 Recommendations of the International Commission on Radiological Protection, Publication 103, Elsevier; 2007.
12. International atomic energy agency, IAEA safety glossary: terminology used in nuclear safety and radiation protection (2007 Edition), IAEA, Vienna; 2007.
13. Jamie M. Shoag, Kevin Michael Burns, Sukhraj S. Kahlon, Patrick J. Parsons, Polly E. Bijur, Benjamin H. Taragin&Morri Markowitz (2020) Lead poisoning risk assessment of radiology workers using lead shields, *Archives of Environmental & Occupational Health*, 2020;75(1):60-64 DOI: 10.1080/19338244.2018.1553843.
14. Balanlı A, Ozturk A, Yapinın İc. Examining indoor and outdoor environments of buildings in terms of building biology. Healthy cities and civilengineering symposium. Chamber of Turkish Civil Engineers, Izmir Branch. 1995;45–55.
15. Ahmmad SK, Jabeen N, Uddin A, Syed T, Ahmed SA, Rahman S. Artificial intelligence density model for oxide glasses, *Ceramics International* 2021;47(6):7946-7956. Available: <https://doi.org/10.1016/j.ceramint.2020.11.144>.
16. Ahmmad, SK, Magudapathy P, Edukondalu A, et al. Nitrogen implantation of zinc arsenic tellurite glasses. *J Aust Ceram Soc*. 2021;57:185–194. Available: <https://doi.org/10.1007/s41779-020-00515-8>.

17. Srinivas B, R. Vijaya R k, Hameed A, Ramadevudu G, M. Narasimha M Chary, Shareefuddin Md. Experimental and theoretical electron paramagnetic resonance and optical studies of Cu²⁺ spin probe in BaO-TeO₂-Bi₂O₃-B₂O₃ glass system, *Optik* 156. 2018;156:289–296.
18. Srinivas B, Srikantha B. Chary , Abdul Hameed , Narasimha M. Chary , Shareefuddin Md. Influence of BaO on spectral studies of Cr₂O₃ doped titanium-boro-tellurite glasses, *Optical Materials* 2020;109:110329.
19. Helena Ticha, Jiri Schwarz, LadislavTichy, Raman spectra and optical band gap in some PbO-ZnO-TeO₂ glasses, *Mater. Chem. Phys.*,2019;237:121834.
20. Gedikoğlu N, Ersundu A, Aydin S, Çelikbilek M. Crystallization behavior of WO₃-MoO₃-TeO₂ glasses, *J. Non-Cryst. Solids*. 2018;501:93–100.
21. TekinHO.,Kassab LRP, OzgeKilicoglu, Evellyn Santos Magalhães, Shams AM, da Silva Mattos GR. Newly developed tellurium oxide glasses for nuclear shielding applications: an extended investigation. *J. Non-Cryst. Solids*. 2019; 10. DIO: 1016/j.jnoncrisol.2019.11976.
22. Sayyed MI, Kawa MK, Gaikwad DK, Agar O, Gawai UP, Baki SO. Physical, structural, optical and gamma radiation shielding properties of borate glasses containing heavy metals (Bi₂O₃/MoO₃) *Journal of Non-Crystalline Solids*, 2019;507:30-37.
23. Chahine A, Et-Tabirou M, Elbenaissi M, Haddad M, Pascal JL. Effect of CuO on the structure and properties of (50-x/2)Na₂O-xCuO-(50-x/2)P₂O₅glasses. *Mater Chem Phys* 2004;84:341-347.
24. Al-Hadeethi Y, Sayyed MI, Mohammed H, Rimondin L. X-ray photons attenuation characteristics for two tellurite-based glass systems at dental diagnostic energies. *Ceram. Int.* 2020;46:251–257.
25. Mhareb M., Almessiere M., Sayyed M. I. and Alajerami Y. Physical, structural, optical and photons attenuation attributes of lithium-magnesium-borate glasses: Role of Tm₂O₃ doping, *Optik*, 2019;182:821-831.
26. Lakshminarayana G, Sayyed MI, Baki SO, Lira A, Dong M, Kawa M, Kaky M, Kityk I and MahdiOptical MA. Absorption and gamma-radiation-shielding parameter studies of Tm³⁺-doped multicomponent borosilicate glasses, *Applied Physics A*, 2018;124:1-16.
27. Şakar E, Özpolat ÖF, Alım B, Sayyed MI, Kurudirek M. Phy-X/PSD: Development of a user-friendly online software for calculation of parameters relevant to radiation shielding and dosimetry. *Radiation Physics and Chemistry*. 2020;166:108496-12.
28. Kıbrıslı O, Ersundu AE, Çelikbilek EM. Dy³⁺ doped tellurite glasses for solid-state lighting: An investigation through physical, thermal, structural and optical spectroscopy studies. *Journal of Non-Crystalline Solids* 2019;513:125-136.
29. Umar SA, Halimah MK, Chan KT, Latif AA., "Physical, structural and optical properties of erbium doped rice husk silicate borotellurite (Er-doped RHSBT) glasses. *J Non Cryst Solids*. 2017;0–1.
30. Hubbell JH, Seltzer SM. Tables of X-Ray Mass Attenuation Coefficients and Mass Energy-Absorption Coefficients 1 keV to 20 MeV for Elements Z=1 to 92 and 48 Additional Substances of Dosimetric Interest. National Institute of Standards and Technology 1995 - PL, Gaithersburg, USA
31. Hubbell JH. Review of photon interaction cross section data in the medical and biological context. *Phys. Med. Biol* 1999;44:R1-R22.
32. Gerward L, GuilbertN, Jensen KB, Levring H. WinXCom - a program for calculating X-ray attenuation coefficients. *Radiat. Phys. Chem* 2004;71:653-654
33. Taylor ML, Smith RL, Dossing F, Franich RD. Robust calculation of effective atomic numbers: the Auto-Z(eff) software. *Med. Phys.* 2012;39:1769-1778.
34. Un at, Caner T. The Direct-Z(eff) software for direct calculation of mass attenuation coefficient, effective atomic number and effective electron number. *Ann. Nucl. Energy* 2014;65:158-165.
35. L.D. Landau, S.I. Pekar. Effective mass of a polaron 2071-0194. *Ukr. J. Phys.* 2008.V. 53, Special Issue, ranslated and reprinted from *Zh. Eksp. Teor. Fiz.* 1948;18(5):419–423.
36. Schott Co: Available: https://www.schott.com/advanced_optics/english/products/optical-materials/special-materials/radiation-shielding-glasses/index.html

37. Kaundal RS. Comparative study of borate glasses. Materials Research. radiation shielding parameters for bismuth 2016;19(4):776-78.

© 2021 Hussein; This is an Open Access article distributed under the terms of the Creative Commons Attribution License (<http://creativecommons.org/licenses/by/4.0>), which permits unrestricted use, distribution, and reproduction in any medium, provided the original work is properly cited.

Peer-review history:
The peer review history for this paper can be accessed here:
<http://www.sdiarticle4.com/review-history/67962>